

**This is a self-archived version of an original article. This version may differ from the original in pagination and typographic details.**

**Author(s):** Ramalho, M.; Suhonen, J.

**Title:** Computed total  $\beta$ -electron spectra for decays of Pb and Bi in the  $^{220,222}\text{Rn}$  radioactive chains

**Year:** 2024

**Version:** Published version

**Copyright:** © 2024 American Physical Society



**Rights:** In Copyright

**Rights url:** <http://rightsstatements.org/page/InC/1.0/?language=en>

**Please cite the original version:**

Ramalho, M., & Suhonen, J. (2024). Computed total  $\beta$ -electron spectra for decays of Pb and Bi in the  $^{220,222}\text{Rn}$  radioactive chains. *Physical Review C*, 109(1), Article 014326.  
<https://doi.org/10.1103/PhysRevC.109.014326>

# Computed total $\beta$ -electron spectra for decays of Pb and Bi in the $^{220,222}\text{Rn}$ radioactive chains

M. Ramalho <sup>1,\*</sup> and J. Suhonen <sup>1,2,†</sup>

<sup>1</sup>*Department of Physics, University of Jyväskylä, P.O. Box 35, FI-40014 Jyväskylä, Finland*

<sup>2</sup>*International Centre for Advanced Training and Research in Physics (CIFRA), P.O. Box MG12, 077125 Bucharest-Magurele, Romania*



(Received 25 September 2023; revised 7 November 2023; accepted 3 January 2024; published 25 January 2024)

The radon radioactivity is an unavoidable background in present and future underground experiments attempting to detect the neutrinoless double  $\beta$  decay, WIMP-nucleus interactions in direct dark-matter searches, etc. In particular, the  $^{220,222}\text{Rn}$  radioactive chains lead to  $\beta^-$  decays of  $^{212,214}\text{Pb}$  and  $^{212,214}\text{Bi}$ , notorious backgrounds in the mentioned experiments. In this paper, we compute the total  $\beta$ -electron spectral shapes of these decays by including next-to-leading-order terms and other correction factors in the  $\beta$  spectral shape. The studied  $\beta^-$  decays involve strong allowed and first-forbidden  $\beta$  transitions, the nonunique first-forbidden transitions being nuclear-structure dependent through the numerous involved nuclear matrix elements (NMEs). We compute these NMEs by using the nuclear shell model with the *khpe* Hamiltonian. This Hamiltonian renders a very nice description of the level energies of the daughter nuclei  $^{212,214}\text{Bi}$  and  $^{212,214}\text{Po}$  of the mentioned mother nuclei. We adopt experimental endpoint energies and engage the small relativistic NMEs (sNME), to accurately describe the measured branching ratios, a necessary prerequisite for a precise description of the total  $\beta$  spectra. We also discuss the uncertainties of our computed spectra and hope that these computations will be of help for present and future rare-decays and dark-matter experiments.

DOI: [10.1103/PhysRevC.109.014326](https://doi.org/10.1103/PhysRevC.109.014326)

## I. INTRODUCTION

$\beta$  decay is a fundamental nuclear process in which a nucleus undergoes a transmutation by emitting a  $\beta$  particle (electron or positron) and a neutrino or antineutrino [1,2]. The study of  $\beta$ -decay spectra provides valuable insights into the underlying nuclear structure and the properties of the involved isotopes. In particular, the investigation of  $\beta$  spectral shapes for isotopes such as  $^{212,214}\text{Pb}$  and  $^{212,214}\text{Bi}$  holds great importance due to their contributions to backgrounds in various scientific measurements, including double- $\beta$ -decay and dark-matter detection experiments.

To accurately interpret experimental data and distinguish potential double- $\beta$  and dark-matter signals from background noise, a comprehensive understanding of the  $\beta$  spectral shapes of isotopes like  $^{212,214}\text{Pb}$  and  $^{212,214}\text{Bi}$  is crucial. These isotopes are part of the background problem emerging from the radon radioactivity, in this case from the  $^{220,222}\text{Rn}$  radioactive chains. The spectral shape refers to the distribution of electron energies emitted in the  $\beta$ -decay process. The total  $\beta$  spectrum is the sum of  $\beta$ -electron spectral shapes corresponding to individual  $\beta$ -decay transitions. Computation of this total spectral shape is quite demanding and experimental  $\beta$ -endpoint energies (in the case of  $\beta^-$  decay the maximum energy of the emitted electron allowed by the available decay energy and its sharing with the emitted electron antineutrino) have to be used. In addition, it should be preferable to reproduce the measured branching ratios as accurately as possible. For the

presently discussed decays, they have been evaluated and can be found in the ENSDF database [3]. The experiment-based evaluated ground-state-to-ground-state endpoint energies ( $Q$  values) vary between  $Q = 0.5691(18)$ – $3.269(11)$  MeV for the discussed nuclei (see the AME2020 database [4]) making the calculation of the total  $\beta$  spectra a challenge since it is quite hard to reliably describe all the decay transitions within  $Q$  windows of this size. As far as we know, there have been only a few attempts to compute total  $\beta$  spectra within decay  $Q$  windows in the range of several MeV, see [5].

In the present computations we use the formalism outlined in [6,7], including the next-to-leading-order terms in the  $\beta$  spectral shape. With this formalism, we are able to compute both the allowed and forbidden transitions involved in the decays  $^{212,214}\text{Pb} \rightarrow ^{212,214}\text{Bi}$  and  $^{212,214}\text{Bi} \rightarrow ^{212,214}\text{Po}$ . The first-forbidden  $\beta$  transitions are particularly important in these decays, consisting of both unique and nonunique transitions. The allowed and unique first-forbidden transitions have universal  $\beta$  spectral shapes but the nonunique transitions depend on nuclear structure through the nuclear matrix elements (NMEs). We compute these NMEs by using the nuclear shell model (NSM) with a well-established Hamiltonian. By varying the value of one of these NMEs, the so-called small relativistic vector NME (sNME) close to its CVC (conserved vector current) value [1], we can reproduce the available data for all the numerous branching ratios involved in the studied total  $\beta$  spectra. In addition, the used Hamiltonian yields quite nice energy spectra within the decay  $Q$  window for the involved daughter nuclei  $^{212,214}\text{Bi}$  and  $^{212,214}\text{Po}$ .

Recent advancements in experimental techniques, such as cryogenic calorimeters and solid-state NMR spectroscopy,

\*madeoliv@jyu.fi

†jouni.t.suhonen@jyu.fi

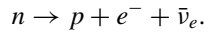
have enabled precise measurements of individual  $\beta$  spectral shapes [8]. These techniques offer high-resolution spectra and improved sensitivity, allowing for a more detailed analysis of the decay process. For instance, the ACCESS (Array of Cryogenic Calorimeters to Evaluate Spectral Shapes) project aims to establish a novel technique for precision measurements of forbidden  $\beta$  decays, which can serve as important benchmarks for nuclear-physics calculations and background studies in astroparticle physics experiments [8]. Individual  $\beta^-$  spectra have already been measured and analyzed for  $^{113}\text{Cd}$  [9–11] and  $^{115}\text{In}$  [12].

The total spectral shapes with multi-MeV  $Q$  windows still offer a grand challenge for the experiments, but the recent advances made in the  $\beta$ -electron detectors [13] offer presently a possibility for the measurements of the total  $\beta$ -electron spectra for  $\beta$  decays with multi-MeV  $Q$  values.

Our article is organized as follows. In Sec. II the adopted theoretical framework is briefly summarized by introducing the  $\beta$ -electron spectral shapes, and the related NMEs and their computation through the NSM. The results are presented and discussed in Sec. III, and the conclusions are drawn in Sec. IV.

## II. THEORETICAL FRAMEWORK

Nuclear  $\beta$  decays are mediated via weak interactions and are a nuclear disintegration process in which the atomic number of the decaying nucleus changes by one. Our current focus involves only  $\beta^-$  decays and it consists of a neutron transmuting into a proton emitting an electron and an electron antineutrino ( $\bar{\nu}_e$ ) within a nuclear environment:



In the following, we describe the theory of  $\beta$ -electron spectral shapes, and the effective values of the weak axial coupling  $g_A$  and weak-axial charge  $g_A(\gamma_5)$ . Furthermore, the NSM, alongside its effective interaction and its model space shall be discussed.

### A. $\beta$ spectral shapes

The branching ratio of a transition to a particular final state in the daughter isotope can be obtained from the corresponding partial half-life which can be written as

$$t_{1/2} = \kappa / \tilde{C}, \quad (1)$$

where  $\kappa = 6289$  s is a collection of natural constants [7] and the integrated shape function reads

$$\tilde{C} = \int_0^{w_0} C(w_e) p w_e (w_0 - w_e)^2 F_0(Z, w_e) dw_e. \quad (2)$$

In this expression,  $F_0(Z, w_e)$ , with  $Z$  as the proton number of the daughter nucleus, is the usual Fermi function taking into account the final-state Coulomb distortion of the wave function of the emitted electron and

$$w_0 = \frac{W_0}{m_e c^2}, \quad w_e = \frac{W_e}{m_e c^2}, \quad p = \frac{p_e c}{m_e c^2} = \sqrt{w_e^2 - 1} \quad (3)$$

are the kinematic quantities scaled dimensionless by the electron rest mass  $m_e c^2$ . Here,  $p_e$  and  $W_e$  are the momentum and energy of the emitted electron, respectively, and  $W_0$  is the  $\beta$

endpoint energy, which for the ground-state transitions defines the  $\beta$ -decay  $Q$  value. The shape factor  $C(w_e)$  contains the Fermi and Gamow-Teller NME for allowed transitions [2] and in general it is a complex combination of leptonic phase-space factors and NME, as described in detail in [1] and recently in [6,14].

For the current work, the main focus involves both first-forbidden unique and nonunique  $\beta^-$  decays. The unique decays have a universal spectral shape, as have the allowed decays, and correspond to  $C(w_e)$  being proportional to a single NME in Eq. (2), as has been extensively discussed in [2]. Higher-forbidden  $\beta$ -decay transitions are strongly suppressed and contribute negligibly to the summed electron spectral shape and are thus not of interest in the current work.

First-forbidden  $\beta$  transitions are associated with tensor operators of rank 0, 1, and 2 [1,15,16]. The pseudotensor  $\Delta J = 2$  transitions with a change in parity are pure axial-vector transitions and include only one NME. These transitions are called first-forbidden unique and have a universal electron spectral shape. The pseudovector  $\Delta J = 1$  and pseudoscalar  $\Delta J = 0$  transitions with a change in parity are transitions that have both vector and axial-vector components and depend on more than one NME, thus being sensitive to details of nuclear structure through the initial and final nuclear wave functions. They are called first-forbidden nonunique. For the vector part and the allowed Fermi transitions, we adopt the CVC-compatible value  $g_V = 1.0$  for the weak vector coupling.

The  $\Delta J = 0$  transitions depend on the weak axial charge  $g_A(\gamma_5)$ , in addition to  $g_A$ . In this work, we will refer to the effective  $g_A^{\text{eff}}$  as simply  $g_A$  and it should not be confused with its free-nucleon value  $g_A^{\text{free}} = 1.27$ . Only these particular transitions and their decay rates depend on the value of the so-called mesonic enhancement factor  $\varepsilon_{\text{MEC}}$ , related to  $g_A$  as follows:

$$g_A(\gamma_5) = \varepsilon_{\text{MEC}} \times g_A. \quad (4)$$

The mesonic enhancement factor with values of  $g_A \approx 0.7$  have been shown to follow the pattern

$$\varepsilon_{\text{MEC}} = 1.576 + 2.08 \times 10^{-3} A \quad (5)$$

in medium to heavy nuclei [17]. For heavy nuclei with a free-nucleon  $g_A$ , the mesonic enhancement factor can be as high as  $\varepsilon_{\text{MEC}} \approx 2.0$ – $2.2$  [18]. However, the magnitude of the mesonic enhancement depends on the model, interaction used, and the selected value of  $g_A$ .

### B. Nuclear shell-model calculations

The NSM calculations were performed using the software KSHELL [19] with the Hamiltonian  $khpe$  [20] found in NuSHELLX@MSU [21]. This interaction and the participant single-particle energies were originally designed to access the level schemes of the mass region  $A = 204$ – $212$  and were also used for  $^{212}\text{Pb}$ , of interest in this work.

The model space consists of the  $^{208}\text{Pb}$  closed core and a valence space consisting of the proton  $\pi(1h_{9/2})$ ,  $\pi(2f_{7/2})$ ,  $\pi(2f_{5/2})$ ,  $\pi(3p_{3/2})$ ,  $\pi(3p_{1/2})$ , and  $\pi(1i_{13/2})$  orbitals and neutron  $\nu(1i_{11/2})$ ,  $\nu(2g_{9/2})$ ,  $\nu(2g_{7/2})$ ,  $\nu(3d_{5/2})$ ,  $\nu(3d_{3/2})$ ,  $\nu(4s_{1/2})$ ,

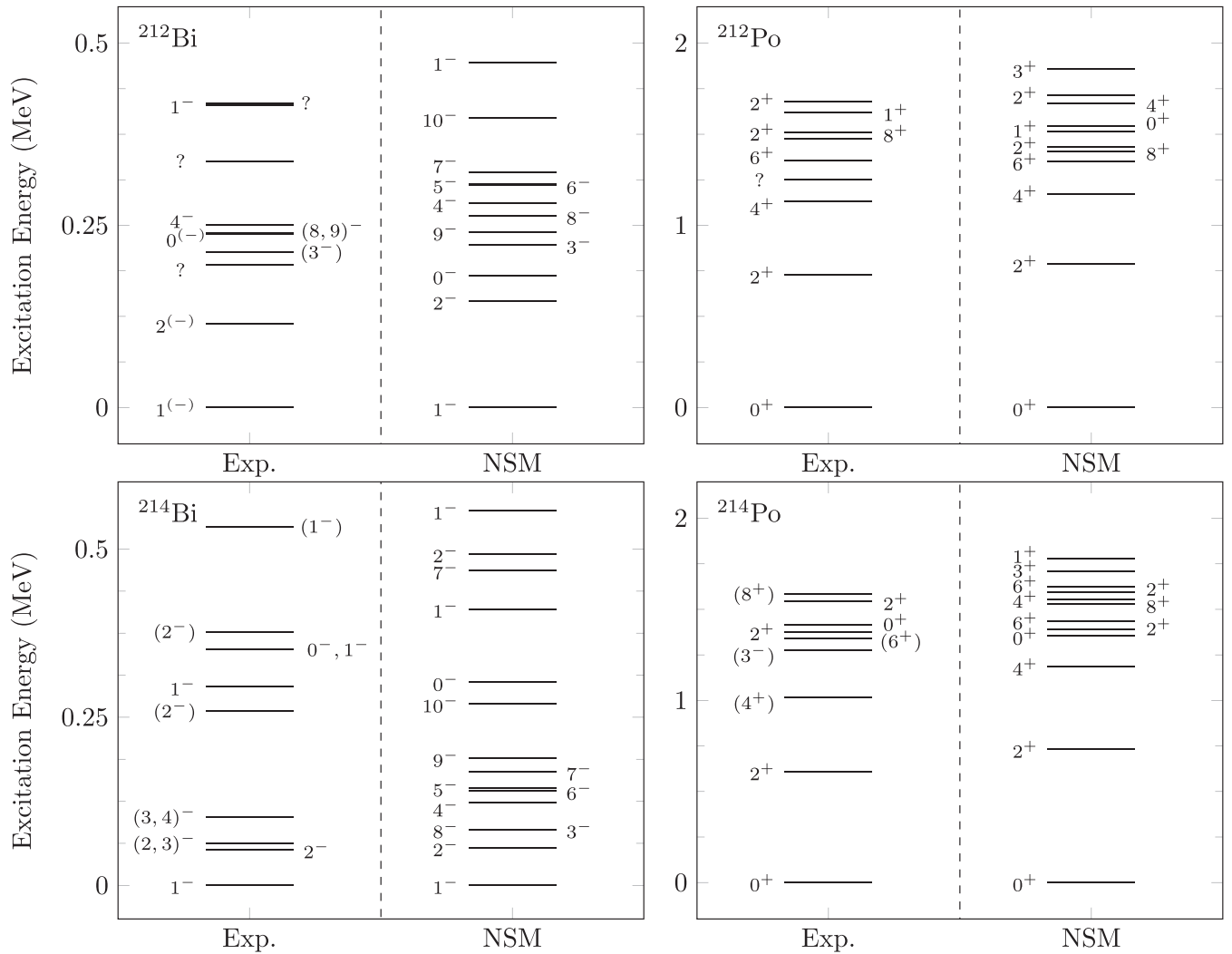


FIG. 1. Computed level schemes for the  $\beta^-$ -decay daughters  $^{212}\text{Bi}$ ,  $^{214}\text{Bi}$ ,  $^{212}\text{Po}$ , and  $^{214}\text{Po}$  using the Hamiltonian  $khpe$ . A comparison with the available data is performed with the parentheses denoting uncertainty in parity and spin-parity assignments. The evaluated data are gathered from [3].

and  $\nu(1j_{15/2})$  orbitals. No truncations were made within the said valence space. This setup enabled us to compute  $^{212}\text{Pb-Bi}$ ,  $^{214}\text{Pb-Bi}$ ,  $^{212}\text{Bi-Po}$ , and  $^{214}\text{Bi-Po}$  level schemes. The daughter level schemes can be seen in Fig. 1.

For  $^{212}\text{Bi}$  ( $^{212}\text{Po}$ ) the energies of the three (four) key levels in terms of  $\beta$  feeding (see Table II) are very well described

TABLE I. Allowed transitions involved in our total  $\beta$ -spectrum analyses. The evaluated [3] branching ratios are reproduced by fitting the values of the Fermi and/or Gamow-Teller NME since the  $\beta$  shapes of allowed decays are universal.

En. (MeV)	$J^\pi$	B.R
$^{214}\text{Pb}(0^+) \rightarrow \text{Bi}$		
0.839	$1^+$	2.75(8)%
$^{214}\text{Bi}(1^-) \rightarrow \text{Po}$		
1.995	$1^-$	1.192(21)%
2.448	$1^-$	2.78(6)%

and the maximum deviation between the experimental and computed level energies is some 60 keV (100 keV), see the upper two panels of Fig. 1 and Table II. For  $^{214}\text{Bi}$  (lower left panel of Fig. 1) the deviation between the experimental and computed energies of the four key levels is below some 150 keV, see Table II. In Table II we have chosen the 351 keV level to be of spin-parity  $0^-$  since it is strongly preferred by the NSM calculation: For the  $^{212}\text{Pb}$  decay the evaluation [3] confirms angular momentum 0 for the daughter state corresponding to the large branching, 81.5%. Similar behavior could be expected for  $^{214}\text{Pb}$ , only two neutrons away from  $^{212}\text{Pb}$ . In addition, the choice of  $0^-$  spin-parity guarantees a match between the numbers of the evaluated and computed  $0^-$  and  $1^-$  states below 0.5 MeV in  $^{214}\text{Bi}$ . Moreover, the choice of the  $0^-$  spin-parity also allows the chosen  $\varepsilon_{\text{MEC}}$  to fit perfectly the branchings of both strong transitions (there is no sNME to be used for the fit, see Table II).

The spectrum of  $^{214}\text{Po}$  (lower right panel of Fig. 1) extends to higher energies than those depicted in Fig. 1. However,

TABLE II. Values of the small vector NME (sNME, columns 5 and 6) for each decay and individual transition (evaluation excitation energy, computed excitation energy, spin-parity of the final state, and the branching to this state are reported in columns 1, 2, 3, and 4, respectively) of interest in this work (i.e., having a non-negligible branching). These values reproduce the experimental branching ratio of the given transition. The numbers with an asterisk (\*) denote the sNME closer to the CVC-predicted one (last column) and are the choice for the crossed-blue curves of Fig 3. The data for the excitation energies are taken from the evaluation [3]. It should be noted that for the  $^{212}\text{Bi}$  decay the total branching to  $\beta^-$  transitions is 64.06%.

Eval. En. (MeV)	Comp. En. (MeV)	$J^\pi$	B.R.	sNME <sup>(1)</sup>	sNME <sup>(2)</sup>	CVC
$^{212}\text{Pb}(0^+) \rightarrow \text{Bi}$						
0.238	0.181	$0^-$	81.5(10)% <sup>a</sup>	—	—	—
0.000	0.000	$1^-$	13.7(10)%	-0.0916	-0.0278*	0.0982
0.415	0.474	$1^-$	5.01(7)%	0.3448*	0.0293	0.6264
$^{214}\text{Pb}(0^+) \rightarrow \text{Bi}$						
0.351	0.302	$0^-$	44.5(7)% <sup>a,c</sup>	—	—	—
0.295	0.411	$1^-$	39.0(5)%	-0.4404*	-0.0890	-0.6002
0.000	0.000	$1^-$	12.7(9)%	-0.1182	-0.0076*	0.0924
0.533	0.673	$1^-$	1.063(18)%	0.0882	-0.0244*	-0.4945
0.259	0.493	$2^-$	0.075(20)% <sup>f</sup>	—	—	—
$^{212}\text{Bi}(1^-) \rightarrow \text{Po}$						
0.000	0.000	$0^+$	55.37(12)%	0.0075*	-0.0261	0.0458
0.727	0.789	$2^+$	4.47(11)%	-0.0209*	-0.0010	-0.0373
1.620	1.515	$1^+$	1.86(4)%	0.0855*	0.0380	0.0709
1.512	1.430	$2^+$	1.44(4)%	0.0844	0.0426*	0.0103
1.806	1.881	$2^+$	0.66(3)% <sup>b</sup>	0.0028	0.0693*	0.0449
$^{214}\text{Bi}(1^-) \rightarrow \text{Po}^e$						
0.000	0.000	$0^+$	19.2(4)%	-0.0080	0.0080*	0.0387
1.729	1.791	$2^+$	17.5(10)%	0.1140*	0.0453	0.0990
1.764	1.780	$1^+$	16.9(11)%	0.0869	0.0376*	0.0498
1.847	1.807	$2^+$	8.16(5)%	-0.0442*	0.0104	-0.0720
1.377	1.390	$2^+$	7.22(8)%	-0.0225*	-0.0523	-0.0298
2.118	2.066	$1^+$	4.33(4)% <sup>b</sup>	0.0489*	0.0124	0.1249
1.543	1.593	$2^+$	3.09(4)% <sup>b</sup>	-0.0361*	-0.0132	-0.0892
2.017	2.026	$0^+$	2.459(15)% <sup>b</sup>	0.0378*	-0.0001	0.0275
2.010	1.994	$2^+$	1.433(11)%	-0.0605*	-0.0324	-0.0501
1.415	1.353	$0^+$	0.90(5)% <sup>b</sup>	0.0232	0.0124*	0.0126
2.204	2.209	$1^+$	5.56(5)% <sup>d</sup>	0.0026	—	0.0101
2.728	2.833	$1^+$	0.542(22)% <sup>d</sup>	-0.0166	—	-0.0675

<sup>a</sup>Fitted to the experimental half-life using only  $\varepsilon_{\text{MEC}}$ . Does not participate in the sNME fitting process.

<sup>b</sup>Transition with beta-spectrum shape independent of the sNME, small branching ratio, or both. Does not contribute to differences in the total spectral shape.

<sup>c</sup>The NSM calculations strongly prefer the spin-parity assignment  $0^-$  out of the two choices  $0^-$ ,  $1^-$  offered by the ENSDF [3] evaluation.

<sup>d</sup>Does not reproduce the ENSDF [3] branching. The value chosen is the one in which the branching is minimized, thus only one sNME value is indicated. NSM branchings are then 7.57% and 2.59%, respectively.

<sup>e</sup>Another 33 transitions were considered in the spectrum and their total branching corresponds to 9.59%, with their major contributions within the electron energies of 0 to 500 keV.

<sup>f</sup>There are no sNME/1-NME values for forbidden unique transitions. The fit was done by changing the associated NME.

we compare the experimental and computed energies of the levels fed by first-forbidden transitions, and relevant for the computation of the total  $\beta$  spectrum, in Table II. From Fig. 1 and Table II one can see that all the measured multipole states  $J^\pi$  below some 1.7 MeV of excitation are described very well by the NSM. In turn, Table II indicates that above 1.7 MeV the correspondence of the computed and experimental energies is still fabulously good. Also, the level schemes for the (grand)mother nuclei  $^{212}\text{Pb}$  and  $^{214}\text{Pb}$  are well described by the presently used Hamiltonian.

After the level schemes were produced for the discussed isotopes, the  $\beta^-$ -decay transitions from the  $^{212}\text{Pb}$ ,  $^{214}\text{Pb}$ ,

$^{212}\text{Bi}$ , and  $^{214}\text{Bi}$ , in their corresponding ground states,  $0^+$ ,  $0^+$ ,  $1^{(-)}$ , and  $1^-$ , to the states of their correspondent daughters  $^{212}\text{Bi}$ ,  $^{214}\text{Bi}$ ,  $^{212}\text{Po}$ , and  $^{214}\text{Po}$ , were computed. All the possible decay transitions from allowed transitions up to first-forbidden unique and nonunique were investigated within the decays  $Q$  windows. Thus, for the decays starting from a  $0^+$  state, the daughter states  $0^{+-}$ ,  $1^{+-}$ ,  $2^-$  were considered, and for the parent nuclei having a  $1^-$  ground state, the daughter states  $0^{+-}$ ,  $1^{+-}$ ,  $2^{+-}$ , and  $3^+$  were included.

We adopted the following  $Q$  values for all our computations:  $Q = 0.5691(18)$ ,  $1.018(11)$ ,  $2.2515(17)$ ,  $3.269(11)$  MeV, respectively, for  $^{212}\text{Pb}$ ,  $^{214}\text{Pb}$ ,  $^{212}\text{Bi}$ , and  $^{214}\text{Bi}$ , as



taken from the mass evaluation [4]. Lastly, for the excited states that most contribute experimentally to the total  $\beta^-$  spectrum, i.e., for those transitions having the highest experimental branching ratios, the computations used the best available endpoint energies by adopting the evaluated excitation energies [3] instead of the computed ones. This was done due to the high  $\beta^-$ -decay rates sensitivity to the available endpoint energy. Here, we note that the allowed decays studied were fit to the experimental branchings by adjusting the values of the Fermi and/or Gamow-Teller NME. This is possible since the  $\beta$  spectral shapes of allowed transitions are universal and thus we can take these decays exactly into account in our total spectral-shape calculations. The spin-parities and branchings of these transitions can be seen in Table I.

### III. RESULTS

Here, we detail the steps involved in the calculations. The predicted decay branchings, partial half-lives, and electron spectral shapes depend on the available endpoint energies, equal to the  $Q$  value for the ground-state transition, taken from the evaluations [3,4] in the present work. There is also a dependence on the values of  $g_A^{\text{eff}}$  and  $\varepsilon_{\text{MEC}}$ , the latter solely for  $\Delta J = 0$  transitions. To have a reasonable theoretical description of the  $\beta$  spectral shapes, one must choose how to best approach systematically the values of  $g_A^{\text{eff}}$  and  $\varepsilon_{\text{MEC}}$ . We have done so in the following manner.

#### A. Determination of the values of the axial couplings

Assessing the proper values of  $g_A^{\text{eff}}$  and  $\varepsilon_{\text{MEC}}$  is rather cumbersome, as reviewed in [16,22]. However, for our current study, previous works shed light on these values. In a previous study Haselschwardt *et al.* [23] performed NSM calculations of the  $\beta$  decay of  $^{214}\text{Pb}$  using the same interaction *khpe*. There, the value of  $g_A^{\text{eff}} = 0.85$  was selected as the most reasonable one and hence we use the same value in the present calculations, as well.

Next, for determining the value of  $\varepsilon_{\text{MEC}}$ , we took the two  $\varepsilon_{\text{MEC}}$ -dependent transitions in  $^{212}\text{Pb}$  and  $^{214}\text{Pb}$ , from  $0^+$  to  $0^-$ , with the experimental branching ratios of 81.5(1)% and 44.5(7)%, respectively, and calculated their half-lives for a range of  $g_A^{\text{eff}} = 0.70$ –1.35, and for  $\varepsilon_{\text{MEC}}$  ranging from 0.8 to 2.7. We then took all the  $(g_A^{\text{eff}}, \varepsilon_{\text{MEC}})$  combinations reproducing the evaluation's partial half-lives for the considered transitions within a relative error of less or equal to 0.1%. The resulting values of these parameters are depicted in Fig. 2. For comparison, the value of the  $(g_A^{\text{eff}}, \varepsilon_{\text{MEC}})$  doublet from a previous analysis, using the value  $g_A = 1.25$ , of Warburton [24], is also shown in the figure. From the curve and its error range, for our choice  $g_A^{\text{eff}} = 0.85$ , we obtain the enhancement-factor range  $\varepsilon_{\text{MEC}} = 2.437 \pm 0.014 \pm 0.003$  (If we consider the uncertainties in  $Q$  value, branching ratio, and total half-life).

#### B. Dependency of the $\beta$ spectral shapes on the value of the sNME

The small relativistic NME, sNME, has been found to play an important role in combined studies of  $\beta$  spectral shapes

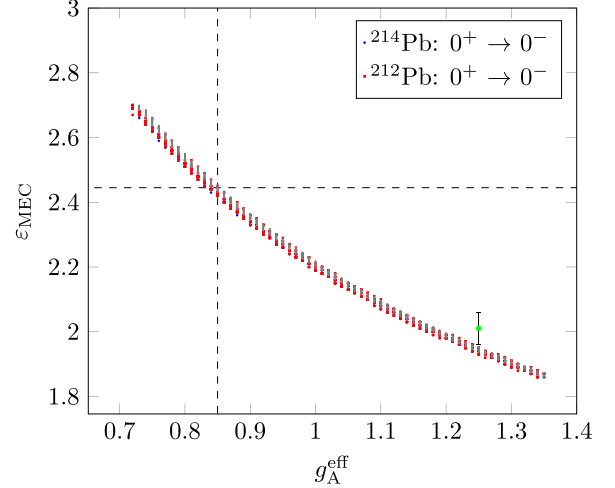


FIG. 2. Value of the enhancement factor  $\varepsilon_{\text{MEC}}$  as a function of  $g_A^{\text{eff}}$  for  $0^+$  to  $0^-$  decays of experimental branchings of 81.5(1)% and 44.5(7)% [3] in  $^{212}\text{Pb}$  and  $^{214}\text{Pb}$ , respectively. Only solutions matching the experimental branchings within 0.1% relative error are plotted. The dashed lines point to our current choice for  $^{214}\text{Pb}$ . The grey dots present the results when uncertainties in the  $Q$  value, branching, and total half-life are considered for the  $^{212}\text{Pb}$  decay. The green dot with its error bars corresponds to the previous analysis of Warburton [24], however, our analysis is not directly comparable to it since in [24] many more transitions than our two were considered.

and branching ratios (partial half-lives) [7,10,11]. In these works the sNME has been used as a fitting parameter, together with  $g_A^{\text{eff}}$  and  $\varepsilon_{\text{MEC}}$  in order to yield both correct beta spectral shapes and branching ratios simultaneously. In the nuclear-structure calculations, the sNME gathers contributions outside the nucleon major shell(s) where the proton and neutron Fermi surfaces lie. Due to the limitation of the NSM valence space to these shells only, the value of the sNME turns out to be zero in the NSM calculations. The value of the sNME cannot be completely arbitrary since in an ideal case (infinite valence spaces, perfect nuclear many-body theory) the value of the sNME is tied to the value of the so-called large vector NME, l-NME, by the CVC (conserved vector current) hypothesis [1]. The value of the l-NME can be rather reliably computed by the NSM since the main contributions to it stem from the major shell(s) where the nucleon Fermi surfaces lie, thus being well accessible for the NSM.

Based on what was said above, one can have a good estimate of the proper value of the sNME by computing its CVC value using the formula (10.69) of [1], where the form factors have been replaced by the NMEs according to the definition (9) of [6], leading to

$${}^v \mathcal{M}_{KK-11}^{(0)} = \left( \frac{(-M_n c^2 + M_p c^2 + W_0) \cdot R}{\hbar c} + \frac{6}{5} \alpha Z \right) \times {}^v \mathcal{M}_{KK0}^{(0)}, \quad (6)$$

where the left side of the equation is the sNME, the last term on the right is the l-NME, and  $K$  denotes the order of forbiddenness, with  $K = 1$  denoting the first-forbidden decays. The quantities  $M_n$  and  $M_p$  denote neutron and proton masses, respectively.  $W_0$  is the available endpoint energy

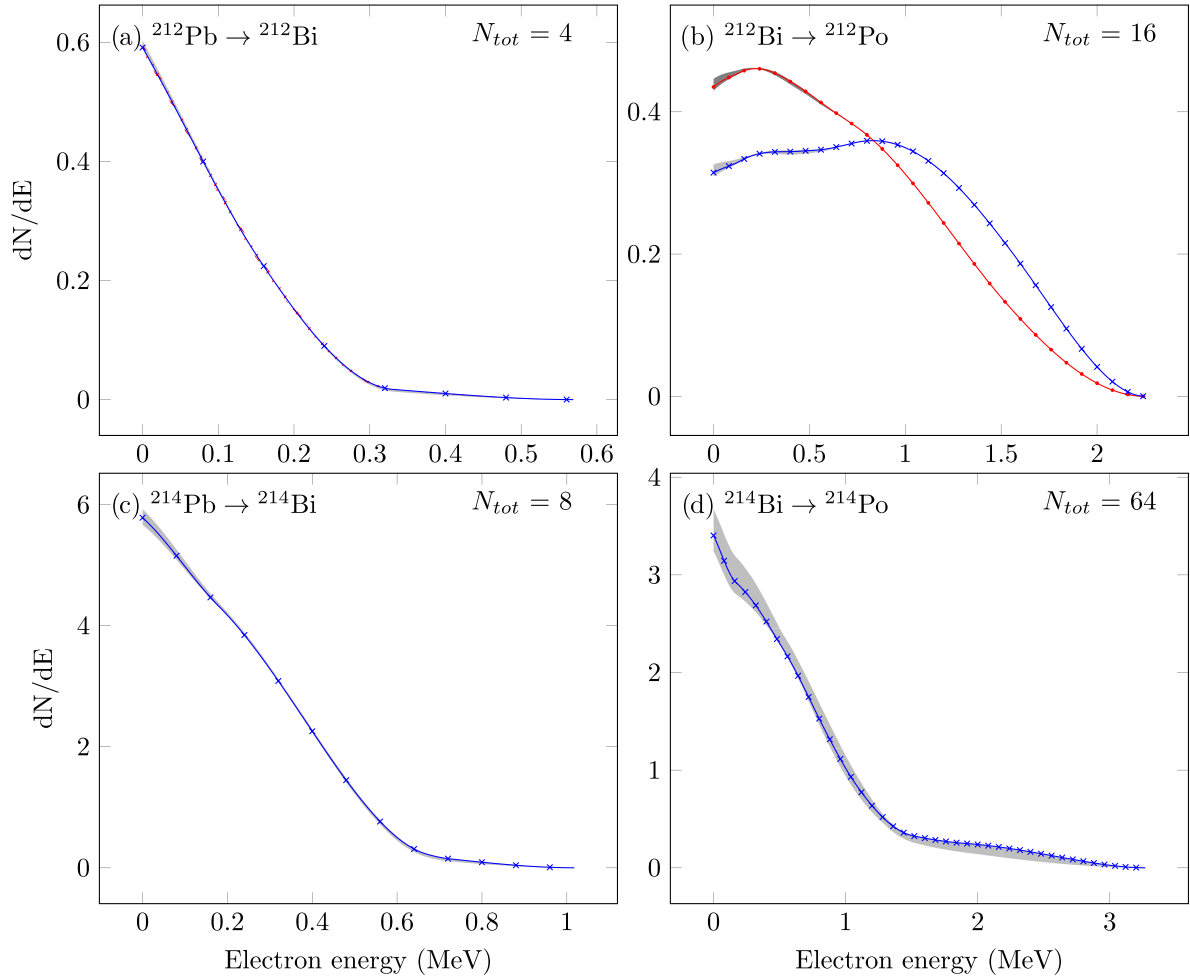


FIG. 3. Computed total  $\beta$  spectra and their dependencies on the choice of the sNME. The crossed-blue curves are those constructed by adopting the value closer to the CVC value for the sNME of an individual transition. The gray-hatched regions denote the span of the curves obtained through the  $N_{\text{tot}}$  (displayed at the top-right corner of each panel) different combinations of the two possible values of sNMEs listed in Table II. The dotted-red curve in (b) uses the value of the sNME further away from its CVC value for the important  $^{212}\text{Bi} \rightarrow ^{212}\text{Po}(\text{g.s.})$  transition, the gray-hatched region being constructed as for the crossed-blue curve. In (a), an error budget, considering the uncertainties of the crossed-blue curve in the  $Q$  value, branchings, and total half-life, is presented by the red-dashed region. These spectral shapes are available from the authors at request. For more information see the text.

for the decay,  $\hbar$  the reduced Planck constant,  $\alpha$  is the fine-structure constant, and  $c$  the speed of light. Lastly,  $Z$  is the atomic number of the daughter nucleus, and  $R = 1.2A^{1/3}$  is the nuclear radius in fm [2],  $A$  being the nuclear mass number.

In our calculations, we adopt the approach of fitting the sNME such that each individual  $\beta^-$  transition with non-negligible experimental branching can be reproduced in terms of the branching ratio. There is a quadratic dependency of the computed branching ratios (partial half-lives) on the value of the sNME and hence two values of the sNME, for each decay transition, reproduce the experimental branching corresponding to this transition. One of these two sNMEs is closer to the CVC value of the sNME and thus offers a way to define the “optimal”  $\beta$  spectral shape: Choosing always the sNME closer to its CVC value produces the most probable total spectral shape, depicted as crossed-blue “CVC” curves in Fig. 3. The

through-the-fit obtained values for the sNMEs are displayed in Table II. As seen in the table, in most cases the selected sNME for the CVC curve is notably closer to the CVC value of sNME than the other solution, making the selection justifiable and the CVC spectrum a robust choice.

The sNME fitting produces two beta spectral curves for each transition. As mentioned above, the CVC curve uses those sNME values closer to their CVC values. The other possible curves are obtained by taking all the  $2^N - 1$  combinations of the values of the sNME,  $N$  denoting the number of transitions considered. The number  $N_{\text{tot}} = 2^N$  is indicated at the top-right corner of each panel of Fig. 3 and ranges from 4 ( $^{212}\text{Pb}$  decay) to 64 ( $^{214}\text{Bi}$  decay, where only the 12 most important transitions as shown in Table II were taken into the sNME variation analysis). Here, it is important to note that all decays in  $^{214}\text{Bi}$  that are energetically allowed and predicted by the NSM are accounted for,

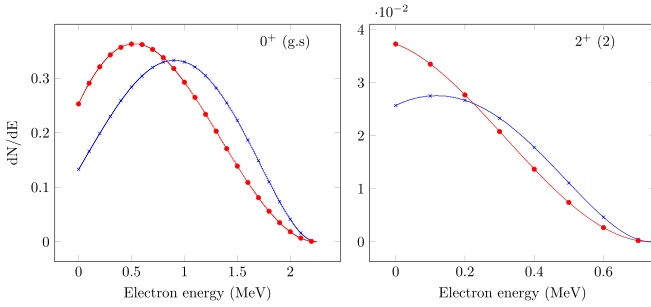


FIG. 4.  $\beta$  spectral shapes of the two transitions that are mostly affected by the choice between the two possible values of the sNME in Table II. These are the transitions from  $^{212}\text{Bi}$  to the ground state (left panel) and the second excited  $2^+$  state (right panel) in  $^{212}\text{Po}$ . The crossed-blue (dotted-red) curve represents the choice closer (farther) from the CVC value of the sNME.

therefore some possibly relevant states, such as those with energies 2.482 MeV (1.192%), 2.192 MeV (0.866%), and 1.890 MeV (1.589%), are accounted for. However, these states were not fitted using the sNME method since their ENSDF spin assignments were not definitive and their energies were not unequivocally predicted by the NSM level schemes so they could not be reliably identified. These states are, instead, included in the 33 transitions that are not displayed in Table II and account for a total of 9.59% of the total half-life.

All the  $2^N$  curves form the gray-hatched region around the “optimal” CVC curve. A notable exception is the decay of  $^{212}\text{Bi}$  where two curves appear in panel b) of Fig. 3. In addition to the crossed-blue CVC curve, there appears a dotted-red curve and its gray-hatched region. This curve is obtained by picking the value  $\text{sNME} = -0.0261$  instead of the value  $\text{sNME} = 0.0075^*$  (which is closer to the CVC value  $\text{sNME} = 0.0458$ ) in the first line of the  $^{212}\text{Bi} \rightarrow ^{212}\text{Po}$  decay in Table II. The gray-hatched region then emerges as in the case of the CVC curve.

The two curves in panel b) of Fig. 3 are presented in order to show that the value of the sNME can have a drastic effect on the  $\beta$  spectral shape. This effect is the strongest for the decay of  $^{212}\text{Bi}$  to the ground state and the second  $2^+$  state (at an excitation energy of 1.512 MeV) in  $^{212}\text{Po}$ , as shown in Fig. 4. In terms of the total  $\beta$  spectrum, panel b) of Fig. 3, the effect of the ground-state transition is the more important one owing to its much larger branching 55.37(12)% as compared to 1.44(4)% of the  $2_2^+$  state.

Lastly, considering the effect of the ENSDF evaluation’s uncertainty in the  $Q$  value, branching ratios, and total half-life on the CVC curve of the  $^{212}\text{Pb} \rightarrow ^{212}\text{Bi}$  decay, as seen in panel a) of Fig. 3, produces a negligible difference in the spectral shape. However, due to the additive nature of experimental uncertainties the effect is expected to be stronger, the more curves the analysis involves and the higher the relative error in the  $Q$  value, making the most susceptible the  $^{212}\text{Bi} \rightarrow ^{212}\text{Po}$  decay due to the 1.080% relative error in the  $Q$  value (versus the 0.3162% for the  $^{212}\text{Pb} \rightarrow ^{212}\text{Bi}$  decay) and  $^{214}\text{Bi} \rightarrow ^{214}\text{Po}$  due to the large number of curves. However, as shown by the error analysis of the  $^{212}\text{Pb} \rightarrow ^{212}\text{Bi}$  decay, we do not

expect that the cumulative effect of the uncertainties in the  $Q$  values, branching ratios, and total half-lives on the presently discussed  $\beta$  spectral shapes are so large as to compete with the uncertainty associated with the selection of the values of the sNME. We have thus omitted the corresponding tedious analyses for the  $^{212,214}\text{Bi}$  and  $^{214}\text{Pb}$  decays.

#### IV. CONCLUSIONS

We believe that the present systematic study of  $\beta$  spectral shapes of key Pb and Bi nuclei in the  $^{220}\text{Rn}$  and  $^{222}\text{Rn}$  chains could be useful to the large underground experiments that struggle with background spectra from these chains. The  $^{222}\text{Rn}$  and  $^{220}\text{Rn}$  nuclei  $\alpha$  decays to  $^{218}\text{Po}$  and  $^{216}\text{Po}$ , which then once again  $\alpha$  decays to  $^{214}\text{Pb}$  and  $^{212}\text{Pb}$ , respectively, and from there the presently studied  $\beta^-$  decays emerge. It is almost impossible to get rid of these contaminants in the rare-events experiments, such as neutrino and dark-matter experiments. The continuous nature of  $\beta^-$  decays and their  $\beta$  electron shapes is a severe challenge in the calibration of the experimental set-ups since one has been relying on software such as GEANT4 [25] with its radioactive decay module or BETASHAPE [26] in the simulations of  $\beta$  decays. The problem with these methods is that they do not take into account the important part played by the nuclear structure in the form of nuclear matrix elements. These softwares can implement measured  $\beta$  spectral shapes but use allowed  $\beta$  shapes or forbidden unique  $\beta$  shapes as surrogates for non-unique decays. This can be dangerous since the non-unique  $\beta$  decays can be extremely dependent on the NMEs and thus affect strongly the calibration of the rare-events experiments.

We believe that the current study can help solve the calibration issue for the  $\beta$  decays of the Pb and Bi nuclei in the  $^{220}\text{Rn}$  and  $^{222}\text{Rn}$  decay chains. This study has inherent uncertainties: The proper values of  $g_A^{\text{eff}}$ ,  $\varepsilon_{\text{MEC}}$ , and sNME. However, for the presently studied  $\beta$  decays there is no strong dependence of the  $\beta$  spectral shapes on the values of  $g_A^{\text{eff}}$  and  $\varepsilon_{\text{MEC}}$ , only the fitted branchings depend on them. The dependence of the  $\beta$  spectral shapes on sNME is there, but it is quite moderate for the decays of  $^{212,214}\text{Pb}$  and  $^{214}\text{Bi}$ , as can be seen in Fig 3, panels (a), (c), and (d). In this figure, panel (b) serves only as an example of the possibility for a large variation of the total spectral shape when even one individual transition, with a large branching, has a strong dependency on the value of the sNME. But even in this case the CVC-based crossed-blue line, with little uncertainty, is the one which should be taken as a paradigm. In any case, our computed spectral shapes make these total  $\beta$  spectra worth studying using experiments like [13]. In addition, the  $\beta$  spectra of individual transitions, listed in Table II, form interesting objects of study using other types of spectral-shape measurements, like ACCESS [8]. By these experiments, a lot can be learned about the appropriate values of the key parameters of  $\beta$ -shape calculations.

Lastly, we note that the present analyses are model dependent: In this case, we use the Hamiltonian *khpe*. However, we believe that this Hamiltonian nicely captures the physics of the involved nuclei, since the level schemes are well reproduced and this particular effective interaction was designed precisely



for the presently studied nuclear region. Further investigations of nuclei and interactions in this particular nuclear region could further shed light on the reliability of the computed  $\beta$  spectral shapes that are important for rare-events experiments.

## ACKNOWLEDGMENT

We acknowledge the support by CSC – IT Center for Science, Finland, for the generous computational resources.

- 
- [1] H. Behrens and W. Bühring, *Electron Radial Wave Functions and Nuclear Beta-Decay*, International Series of Monographs on Physics (Clarendon Press, Oxford, UK, 1982).
- [2] J. Suhonen, *From Nucleons to Nucleus: Concepts of Microscopic Nuclear Theory* (Springer-Verlag, Berlin/Heidelberg and Springer, Gaithersburg MD, 2007).
- [3] From ENSDF database as of Nov. 2023, version available at <http://www.nndc.bnl.gov/ensarchivals/>.
- [4] M. Wang, W. Huang, F. Kondev, G. Audi, and S. Naimi, *Chin. Phys. C* **45**, 030003 (2021).
- [5] M. Ramalho, J. Suhonen, J. Kostensalo, G. A. Alcalá, A. Algora, M. Fallot, A. Porta, and A.-A. Zakari-Issoufou, *Phys. Rev. C* **106**, 024315 (2022).
- [6] M. Haaranen, J. Kotila, and J. Suhonen, *Phys. Rev. C* **95**, 024327 (2017).
- [7] A. Kumar, P. C. Srivastava, and J. Suhonen, *Eur. Phys. J. A* **57**, 225 (2021).
- [8] L. Paganini, G. Benato, P. Carniti, E. Celi, D. Chiesa, J. Corbett, I. Dafinei, S. Di Domizio, P. Di Stefano, S. Ghislandi *et al.* (ACCESS Collaboration), *Eur. Phys. J. Plus* **138**, 445 (2023).
- [9] L. Bodenstern-Dresler, Y. Chu, D. Gehre, C. Gössling, A. Heimbald, C. Herrmann, R. Hodak, J. Kostensalo, K. Kröniger, J. Küttler *et al.* (COBRA Collaboration), *Phys. Lett. B* **800**, 135092 (2020).
- [10] J. Kostensalo, J. Suhonen, J. Volkmer, S. Zatschler, and K. Zuber, *Phys. Lett. B* **822**, 136652 (2021).
- [11] J. Kostensalo, E. Lisi, A. Marrone, and J. Suhonen, *Phys. Rev. C* **107**, 055502 (2023).
- [12] A. F. Leder, D. Mayer, J. L. Ouellet, F. A. Danevich, L. Dumoulin, A. Giuliani, J. Kostensalo, J. Kotila, P. de Marcillac, C. Nones, V. Novati, E. Olivieri, D. Poda, J. Suhonen, V. I. Tretyak, L. Winslow, and A. Zolotarova, *Phys. Rev. Lett.* **129**, 232502 (2022).
- [13] V. Guadilla, A. Algora, M. Estienne, M. Fallot, W. Gelletly, A. Porta, L.-M. Rigalleau, and J.-S. Stutzmann, [arXiv:2305.13832](https://arxiv.org/abs/2305.13832) [physics.ins-det].
- [14] M. Haaranen, P. C. Srivastava, and J. Suhonen, *Phys. Rev. C* **93**, 034308 (2016).
- [15] H. Ejiri, J. Suhonen, and K. Zuber, *Phys. Rep.* **797**, 1 (2019).
- [16] J. T. Suhonen, *Front. Phys.* **5**, 55 (2017).
- [17] J. Kostensalo and J. Suhonen, *Phys. Lett. B* **781**, 480 (2018).
- [18] K. Kubodera and M. Rho, *Phys. Rev. Lett.* **67**, 3479 (1991).
- [19] N. Shimizu, T. Mizusaki, Y. Utsuno, and Y. Tsunoda, *Comput. Phys. Commun.* **244**, 372 (2019).
- [20] E. K. Warburton and B. A. Brown, *Phys. Rev. C* **43**, 602 (1991).
- [21] B. A. Brown and W. D. M. Rae, *Nucl. Data Sheets* **120**, 115 (2014).
- [22] J. Suhonen and J. Kostensalo, *Front. Phys.* **7**, 29 (2019).
- [23] S. J. Haselschwardt, J. Kostensalo, X. Mougeot, and J. Suhonen, *Phys. Rev. C* **102**, 065501 (2020).
- [24] E. K. Warburton, *Phys. Rev. C* **44**, 233 (1991).
- [25] S. Agostinelli, J. Allison, K. Amako, J. Apostolakis, H. Araujo, P. Arce, M. Asai, D. Axen, S. Banerjee, G. Barrand *et al.*, *Nucl. Instrum. Methods Phys. Res. A* **506**, 250 (2003).
- [26] X. Mougeot, *Appl. Radiat. Isot.* **201**, 111018 (2023).